The Astronomical Journal, 145:126 (9pp), 2013 May doi:10.1088/0004-6256/145/5/126
© 2013. The American Astronomical Society. All rights reserved. Printed in the U.S.A.

EFFICIENT SELECTION AND CLASSIFICATION OF INFRARED EXCESS EMISSION STARS BASED ON *AKARI* AND 2MASS DATA

Ya Fang Huang[1], Jin Zeng Li[1], Travis A. Rector[2], and Carlos C. Mallamaci[3]
[1] National Astronomical Observatories, Chinese Academy of Sciences, 20A Datun Road, Chaoyang District, Beijing 100012, China; ljz@nao.cas.cn
[2] University of Alaska, 3211 Providence Drive, Anchorage, AK 99508, USA
[3] Observatorio Astronómico Félix Aguilar, Universidad Nacional de San Juan, Argentina
Received 2012 July 17; accepted 2013 February 26; published 2013 March 25

ABSTRACT

The selection of young stellar objects (YSOs) based on excess emission in the infrared is easily contaminated by post-main-sequence stars and various types of emission line stars with similar properties. We define in this paper stringent criteria for an efficient selection and classification of stellar sources with infrared excess emission based on combined Two Micron All Sky Survey (2MASS) and *AKARI* colors. First of all, bright dwarfs and giants with known spectral types were selected from the *Hipparcos* Catalogue and cross-identified with the 2MASS and *AKARI* Point Source Catalogues to produce the main-sequence and the post-main-sequence tracks, which appear as expected as tight tracks with very small dispersion. However, several of the main-sequence stars indicate excess emission in the color space. Further investigations based on the SIMBAD data help to clarify their nature as classical Be stars, which are found to be located in a well isolated region on each of the color–color (C–C) diagrams. Several kinds of contaminants were then removed based on their distribution in the C–C diagrams. A test sample of Herbig Ae/Be stars and classical T Tauri stars were cross-identified with the 2MASS and *AKARI* catalogs to define the loci of YSOs with different masses on the C–C diagrams. Well classified Class I and Class II sources were taken as a second test sample to discriminate between various types of YSOs at possibly different evolutionary stages. This helped to define the loci of different types of YSOs and a set of criteria for selecting YSOs based on their colors in the near- and mid-infrared. Candidate YSOs toward IC 1396 indicating excess emission in the near-infrared were employed to verify the validity of the new source selection criteria defined based on C–C diagrams compiled with the 2MASS and *AKARI* data. Optical spectroscopy and spectral energy distributions of the IC 1396 sample yield a clear identification of the YSOs and further confirm the criteria defined for exploring the nature and properties of unknown excess emission sources in the infrared without optical identification.

Key words: H II regions – stars: early-type – stars: formation – stars: pre-main sequence – stars: variables: T Tauri, Herbig Ae/Be

Online-only material: color figures

1. INTRODUCTION

The development of technology and observational instruments in the infrared (IR) in recent decades fostered various ground- and space-based sky surveys in the near- to far-IR. The pioneering *InfraRed Astronomical Satellite* (*IRAS*) was successfully launched in the 1990s. Its all-sky survey covers more than 96% of the entire sky in four photometric bands at 12, 25, 60, and 100 μm. The IRAS Sky Survey Atlas has shown that mid- and far-IR census is essential for investigations of dusty embedded objects. However, its spatial resolution is comparatively low and not suitable for studying sources in crowded regions. The Two Micron All Sky Survey (2MASS) is the first near-IR survey that made uniformly calibrated observations of the entire sky in the J (1.25 μm), H (1.65 μm), and K_S (2.16 μm) bands with a pixel size of 2″.0. Sources brighter than about 1 mJy in each band were detected with a signal-to-noise ratio greater than 10, which leads to a photometric completeness to 15.9, 15.0, and 14.3 mag, respectively, for each band in unconfused regions. Therefore, 2MASS provides an opportunity to investigate sources with near-IR excess emission. However, the excesses of many YSOs are difficult to detect at K_S and thus longer-wavelength observations are needed. This prevents an efficient search for objects surrounded by dust. *AKARI*, a satellite operated by Japan, fulfills the need for a new mid- and far-IR whole sky survey with better sensitivity and higher spatial resolution. Since it launched on 2006 February 21, *AKARI* has mapped 96% of the entire sky in mid- and far-IR using two on-board instruments: the InfraRed Camera (IRC; Onaka et al. 2007) and Far-Infrared Surveyor (FIS; Kawada et al. 2007). The FIS swept about 94% of the whole sky more than twice at 65, 90, 140, and 160 μm wavebands, while IRC swept more than 90% of the whole sky more than twice using two filter bands centered at 9 μm (*S9W*; 7–12 μm) and 18 μm (*L18W*; 14–25 μm) (Ishihara et al. 2010). The pixel scale of the survey mode of observation is about 10 arcsec pixel^{-1}, and the positional accuracy is better than 3 arcsec.

A large majority of young stellar objects (YSOs) present excess emission in the IR, which is usually interpreted in terms of the presence of a circumstellar disk or dusty envelope. We focus on the selection and classification of sources with excess emission based on archived 2MASS and *AKARI* data. This leads to the introduction of effective new source selection criteria. IR excess emission sources are selected as candidate YSOs such as T Tauri stars (TTS) and Herbig Ae/Be stars (HAeBe). TTS are low-mass (up to 3 $M_{\odot}$), late spectral type (later than mid-F), and variable pre-main-sequence (PMS) stars with a relatively young age (from 10^5 yr to a few 10^7 yr). TTS can be further classified into weak-line TTS (WTTS; low-mass PMS with a spectral energy distribution (SED) well resembling their main-sequence (MS) counterpart), classical TTS (CTTS; low-mass PMSs indicating strong Hα and various forbidden emission lines and signatures of veiling in their optical spectra), and transition objects defined by Sicilia-Aguilar et al. (2006b;

low-mass PMSs showing IR excess only at the longer wavelengths at the intermediate stage between CTTS and WTTS).

HAeBe, on the other hand, are PMSs of spectral types A, B, or early F with signatures of strong hydrogen and calcium emission lines. Color–color (C–C) diagrams in especially the near-IR have been widely used in the past in the selection of YSOs; however, various types of YSOs with excess emission used to be located at similar loci in the near-IR color space and hard to distinguish between each other.

The advent of the *AKARI* All Sky Survey makes it possible to further employ mid-IR colors in the investigation of YSOs. In this paper, we define specific regions on near- to mid-IR C–C diagrams for YSOs with different evolutionary status. Wavelength dependence of interstellar extinction in 2MASS (J, H, and K_S) and *AKARI* IRC ($S9W$ and $L18W$) bands and intrinsic colors for dwarfs in the mid-IR are also calculated.

IC 1396 is a shell-like H II region associated with Trumpler 37 (Tr 37), a very young open cluster (Kun et al. 2008) with an age of 4 Myr (Sicilia-Aguilar et al. 2005) that is located at the southwest tip of Cepheus OB2, just above the Galactic plane at $l = 99^\circ\!.3$ and $b = 3^\circ\!.74$. This H II region is mainly excited by the central O6 star HD 206267, which is a trapezium system (Abt 1986). As an extended H II region ($\sim 3^\circ$) at about 800 pc (Simonson 1968), it comprises a wealth of PMS that makes it a primary target for the study of star formation activities. In this paper, IR excess emission sources toward IC 1396 were employed to verify our new source selection criteria. Optical spectroscopy and SED fitting of the sample sources yield a clear identification of the YSOs and help to confirm the validity of the source selection criteria.

The paper is organized as follows. We present in Section 2 the retrieval of archived 2MASS and *AKARI* data, optical spectroscopy, and its data reduction. In Section 3, we define based on the high-quality data the IR excess emission source selection and classification criteria, and verification of which is given in Section 4. Then the results achieved are discussed and summarized in Section 5.

2. DATA ACQUISITION AND ANALYSIS

2.1. Archival Data

Archived data from the 2MASS Point Source Catalog (PSC) were used in our work. To guarantee the reliability of the data, we employed the following strict requirements in the sample selection, which are revised based on the criteria presented by Li & Smith (2005a): (1) each source extracted from the 2MASS PSC must have certain detection in all JHK_S bands (this directly constrains the $[JHK_S]_{cmsig}$ option to less than or equal to 0.1). (2) Only sources with a K_S-band signal-to-noise ratio above 15 are selected.

The sample of excess emission sources selected based on the 2MASS data is cross-identified with the *AKARI* (ASTRO-F) IRC PSC[4] with a tolerance radius of 3″ (Ita et al. 2010). If more than one *AKARI* source are found within the tolerance radius, only the closest one is adopted. Only sources with both valid $S9W$ and $L18W$ data ($f_{\rm Qual}09 = 3$ and $f_{\rm Qual}18 = 3$) were considered. The flux of IRC PSC sources were then converted to apparent magnitude with the following equation:

$$M - M_0 = -2.5 \times \log_{10}\left(\frac{\rm Flux}{\rm Flux_0}\right)$$

where $\rm Flux_0$ (zero magnitude flux) is 56.262 ± 0.8214 Jy and 12.00 ± 0.1751 Jy for 9 μm and 18 μm bands, respectively.

2.2. Optical Spectroscopy

Spectroscopic observations of all the IC 1396 sample sources with USNO R magnitudes brighter than 17.0 were undertaken on the 2.16 m optical telescope of the National Astronomical Observatories of the Chinese Academy of Sciences. The OMR (Optomechanics Research, Inc.) and the detector PI 1340 × 400 CCD were used in both runs of observations. The low-resolution spectroscopy (with dispersion of 200 Å mm^{-1}, 4.8 Å pixel^{-1}, and 2″.5 slit) centered at 6300 Å has been carried out on 2009 September 12, December 11, and 2010 October 3 and 4.

The spectral data were reduced following standard procedures in the NOAO Image Reduction and Analysis Facility (IRAF, version 2.11) software packages. The CCD reduction includes bias and flat-field correction, nebular and sky background subtraction, and cosmic-ray removal. Wavelength calibration was performed based on helium–argon lamps exposed at both the beginning and the end of the observations each night. Flux calibration of each spectrum was conducted based on observations of at least two of the Kitt Peak National Observatory (KPNO) spectral standards (Massey et al. 1988) each night. The atmospheric extinction is corrected by the mean extinction coefficients measured for the Xing-Long Station, where the 2.16 m telescope is located, by the Beijing–Arizona–Taiwan–Connecticut multicolor survey.

We use Hα as a signpost for classifying YSOs. The inhomogeneous nebular emission in star-forming regions could confuse the observed Hα line from YSOs (Sicilia-Aguilar et al. 2004). Therefore, background subtraction was carefully carried out to avoid the over or undersubtraction of nebular Hα. Taking the treatment of source No. 4 (as listed in Table 3) for instance, we illustrate the process of background subtraction in detail. In Figure 1, the Hα narrowband image around this source from the KPNO Mayall 4 m telescope is shown. The targeted source is indicated with a large cross symbol. The $5' \times 5'$ field of view of 2.16 m telescope is marked with a box. The vertical thick line labels the position of the slit. Note that nebular Hα emission was evidently detected in the vicinity of NO. 4 source. So, it is crucial to carefully select appropriate ambient as representative of background emission. A reasonable principle is to mark the nearest smooth regions on both sides of the source along the slit direction as sky background. The black bars in Figure 1 are used to restrict two small regions with emission. By using this method we are confident that the measured intensity of the Hα line originates from the target source.

Spectral types were then derived with software that can automatically classify spectral types by comparing the ratios of well-defined He I lines to Hβ and standard stars listed in Jacoby et al. (1984). The mainly used lines are He I 4471 Å, 4992 Å, 5876 Å, Mg I 5169 Å, and Ca I 6162 Å. Based on the statistical analysis of the spectral standard stars, the estimated errors are about 1–2 subtypes.

2.3. Narrowband Imaging

Narrowband imaging of IC 1396 was carried out with the MOSAIC camera on the Mayall 4 m telescope at KPNO. MOSAIC is an optical camera that consists of eight 2048×4096 CCD detectors arranged to form a 8192×8192 array with 35 to 50 pixel wide gaps between the CCDs. At the time of the observations, MOSAIC was equipped with thinned, science-grade SITe CCD cameras. With a scale of 0″.26 pixel^{-1}, the

[4] http://darts.isas.jaxa.jp/astro/akari/cas.html

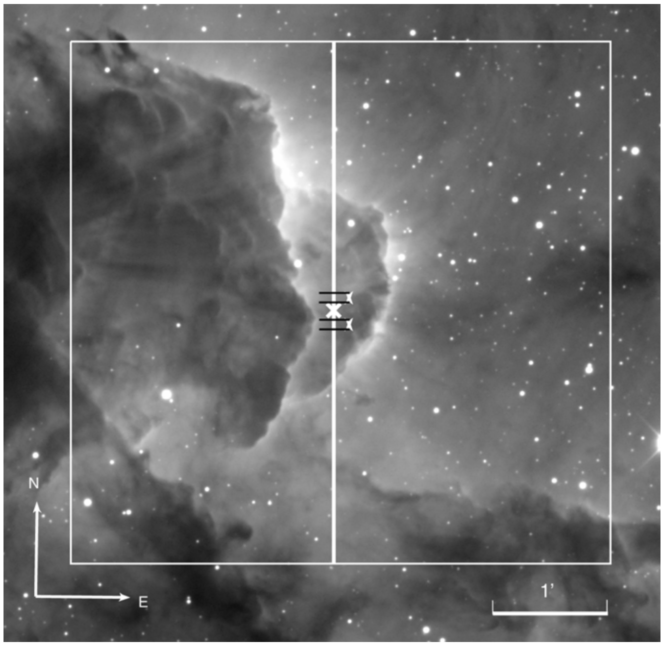

Figure 1. Field of the spectroscopy with the 2.16 telescope of NAOC. The white box indicates the field of view with a physical scale of $5' \times 5'$. The central plus shows the position of the target source, the thick line in the middle shows the overlaid slit position, and the sky background deployed in the spectroscopic data reduction was marked by two pairs of black lines on each side of the source position. The background image is the Hα band image taken by the KPNO 4 m telescope.

field of view is approximately $36' \times 36'$. To fill in the gaps and bad columns, all observations are completed in a five-exposure dither pattern with offsets of approximately 100 pixels.

Observations toward IC1396 were obtained on 2011 October 10 with the Hα (k1009) filter, whose central wavelengths/FWHMs are 6574.74/80.62 and five exposures of 300 s were obtained.

3. METHODOLOGY

Test samples of various types of known YSOs cross-identified with archived 2MASS and *AKARI* data were plotted onto the C–C diagrams to facilitate the selection and classification of IR excess emission sources.

3.1. Main-sequence Stars and Classical Be Stars

First of all, a set of bright dwarfs and giants with known spectral types were selected from the *Hipparcos* Catalogue to compile the MS and the post-MS star tracks. To guarantee that the intrinsic color of the MS can be accurately depicted, except for the limit on photometric accuracy (standard error of the B magnitude $\delta B_T < 0.05$ and standard error of the V magnitude $\delta V_T < 0.05$), an additional limit on color ($-0.5 \leqslant B - V \leqslant 2.0$) was also omitted sources with likely uncertain spectral classification. Then the sample of known giants and dwarfs were cross-identified with the 2MASS PSC and *AKARI* IRC PSC and put onto various testing C–C diagrams. Based on the distribution of the MS and post-MS stars, $(J-H)$ versus $(H-K_S)$ (hereafter JHK_S), $(J-K_S)$ versus $(K_S - S9W)$ (hereafter $JK_S[9]$) and $(K_S - S9W)$ versus $(S9W - L18W)$ (hereafter $K_S[9][18]$) (Figure 2) were found to be more appropriate in the selection and classification of IR excess emission sources.

Table 1 presents the wavelength dependence of interstellar extinction, which helps to define the reddening band in the color

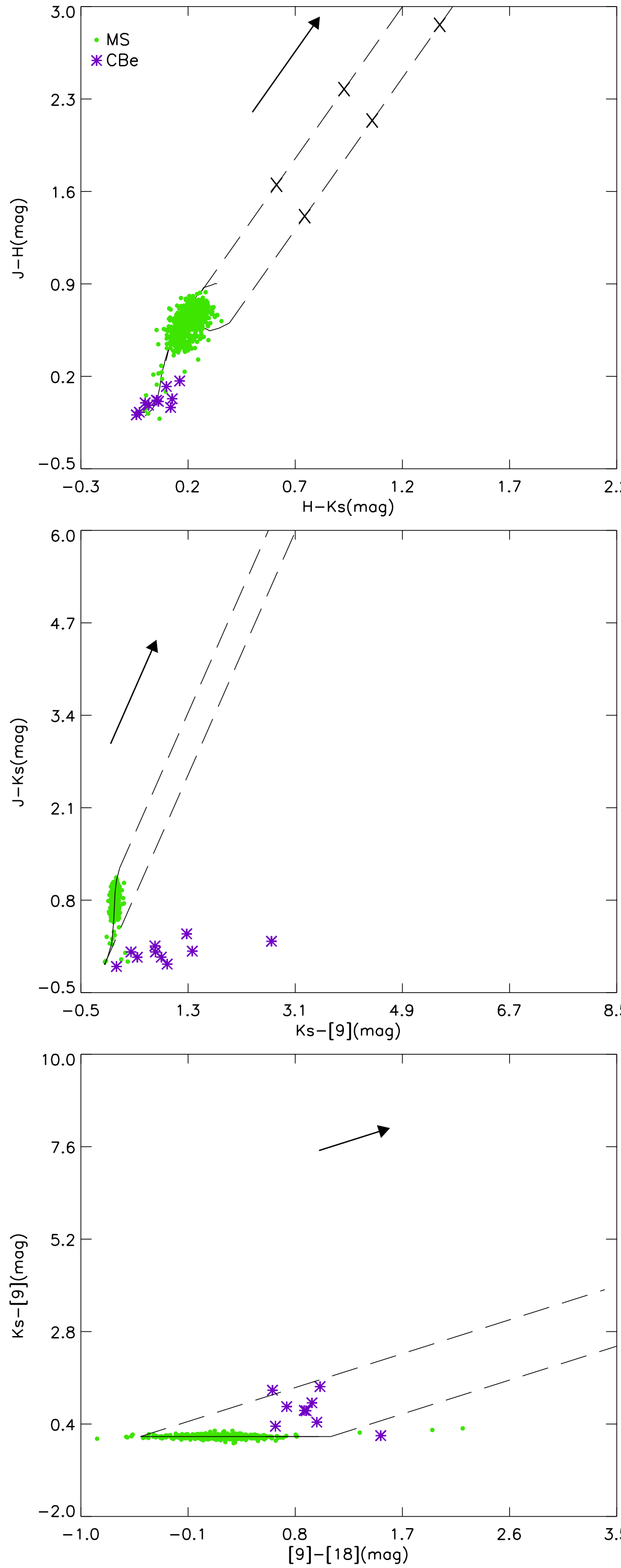

Figure 2. Distribution of the MS and post-MS sources in C–C diagrams. The tracks of them shown in solid lines were compiled from high-precision data from the *Hipparcos* Main Catalog. The symbols in the three diagrams are the same. Green dots and purple asterisk represent normal stars and CBe, respectively. Long dashed lines delineate the reddening band for normal stars. The arrow shows a reddening vector of $A_v = 5$ mag (Rieke & Lebofsky 1985) in JHK_S and $A_v = 10$ mag in $JK_S[9]$ and $K_S[9][18]$.

(A color version of this figure is available in the online journal.)

Table 1
Wavelength Dependence of Interstellar Extinction in the 2MASS (J, H, K_S) and *AKARI* IRC ($S9W$ and $L18W$) Bands

Band	Wavelength (μm)	A_λ/A_V
J	1.25	0.282
H	1.65	0.175
K_S	2.17	0.128
$S9W$	9	0.081
$L18W$	18	0.048

space. The wavelength dependence of extinction in the 2MASS bands is calculated from the distribution of the reddened MS stars toward IC 1396, and that for the *AKARI* bands is adopted from results in the literature (Rieke & Lebofsky 1985; Draine 2003).

In Figure 2, the distribution of the MS and post-MS stars shown as solid lines seem to evolve with wavelength in the color space. The high-quality data employed in this study result in similar MS and post-MS tracks in the JHK_S diagram, which, however, appear as neat and tight tracks in the $JK_S[9]$ diagram (data points of the fit curve are shown in Table 2) and yield nearly perfect tracks with very small dispersion in the $K_S[9][18]$ diagram (following strictly a horizontal line with $(K_S - S9W) = 0.75$). The reddening band of the MS and post-MS stars in the mid-IR C–C diagrams is defined based on their distribution and the reddening vector. Neat MS and post-MS tracks are the critical basis for the classification of various types of excess emission sources in the IR. As a case in this study, several sources in the MS sample (marked as purple asterisks) indicate marginal excess emission in the JHK_S diagram. However, they are found to occupy well isolated loci in the $JK_S[9]$ and $K_S[9][18]$ diagrams. Detailed investigation based on the SIMBAD database revealed their origin as classical Be stars (CBe). This confirms, on the other hand, the neatness of the MS and the post-MS tracks and likely validity of the source selection criteria defined in this paper.

3.2. Removal of Major Contaminants

Two test samples of YSOs were employed to investigate potential clues to discriminate between various types of YSOs. The first test sample consists of 92 candidate HAeBe adopted from Thé et al. (1994) and CTTSs from the Herbig–Bell Catalogue.[5] And the second one contains of Class I and Class II sources classified by Gutermuth et al. (2008, 2009).

For the reliable selection of genuine YSOs, the distribution of various types of major contaminants have to be investigated and removed. The samples of potential major contaminants were adopted from Gutermuth et al. (2008, 2009) and Takita et al. (2010). The color properties of the following samples of contaminants were examined: (1) a sample of asymptotic giant branch (AGB) stars consisting of 126 carbon and 563 OH/IR stars (Le Bertre et al. 2003), (2) a sample of 1143 planetary nebulae (PNe; Acker et al. 1994), and (3) a set of 146 extragalactic objects extracted from the north and south equatorial poles (Koenig et al. 2012). All the contaminating sources were cross-identified with the 2MASS catalog and the *AKARI* IRC PSC and then plotted onto the C–C diagrams in Figure 3.

[5] http://www.stsci.edu/~welty/HBC/HBC.html

Table 2
Calculated Dwarfs and Giants Tracks Based on Their Distribution in the $JK_S[9]$ C–C Diagram

$K_S - S9W$	$J - K_S$
−0.1	−0.1
−0.05	0
0.02	0.2
0.05	0.5
0.075	0.92
0.1	1.08
0.15	1.25

Based on their distribution in the color space, candidate PNe meet the following color constraints:

$$(K_S - S9W) + 1.023 \times (S9W - L18W) - 9.313 > 0$$
$$S9W - L18W > 2.75.$$

OH/IR stars were found to follow the criteria shown below:

$$1.069 < (K_S - S9W) + 0.062 \times (S9W - L18W) < 2.569.$$

And criteria for the selection of carbon stars are as follows:

$$(K_S - S9W) - 0.978 \times (S9W - L18W) - 0.564 > 0$$
$$S9W - L18W < 1.$$

The removal of contaminated star-forming galaxies from our sample is similar to the *WISE* studies by Koenig et al. (2012). The corresponding *AKARI* photometric data were extracted from the north and south equatorial poles (decl. $> +88^\circ\!.22$ and also decl. $< -88^\circ\!.22$), which were assumed to consist mostly of galaxies. Based on their distribution in the $K_S[9][18]$ C–C diagram (Figure 3), they can be successfully removed with the same criteria as those for carbon stars.

Based on detailed investigation of TTS stars with *AKARI* by Takita et al. (2010), post-AGB stars are not major contaminants to the selection of TTS. Potential contamination from post-AGB is, therefore, not considered in this paper.

3.3. Young Stellar Objects

The two test samples of YSOs were then plotted onto the C–C diagrams in order to investigate potential clues to discriminate between various types of YSOs. After cross-identification with the 2MASS catalog and the *AKARI* IRC PSC, the first test sample consists of 92 candidate HAeBe and 154 CTTSs. They were plotted onto the different C–C diagrams in Figure 4.

In Figure 4, the majority of the CTTSs are found to be congregated to the right of the reddening band for normal stars on the JHK_S diagram. While all of the HAeBe are located to the right of the CTTSs. Based on the distribution of the sample sources, a dot-dashed division line is defined between the loci of CTTSs and HAeBe. Therefore, JHK_S diagram appears to be more efficient in the classification of CTTS and HAeBe. In the $JK_S[9]$ diagram, CTTS and HAeBe are mixed together, but the distribution of them shows a clear cut in the color space. We define here a tentative line, parallel to the reddening band of normal stars, to delineate the left edge of the distribution of YSOs in $JK_S[9]$. However, the distribution of test sample in $K_S[9][18]$ is much different from that in the JHK_S and $JK_S[9]$ diagrams. Almost all the CTTS and HAeBe are found to be located above the reddening band and there seems to exist a clear cut on the left of them. A dot-dashed line is therefore

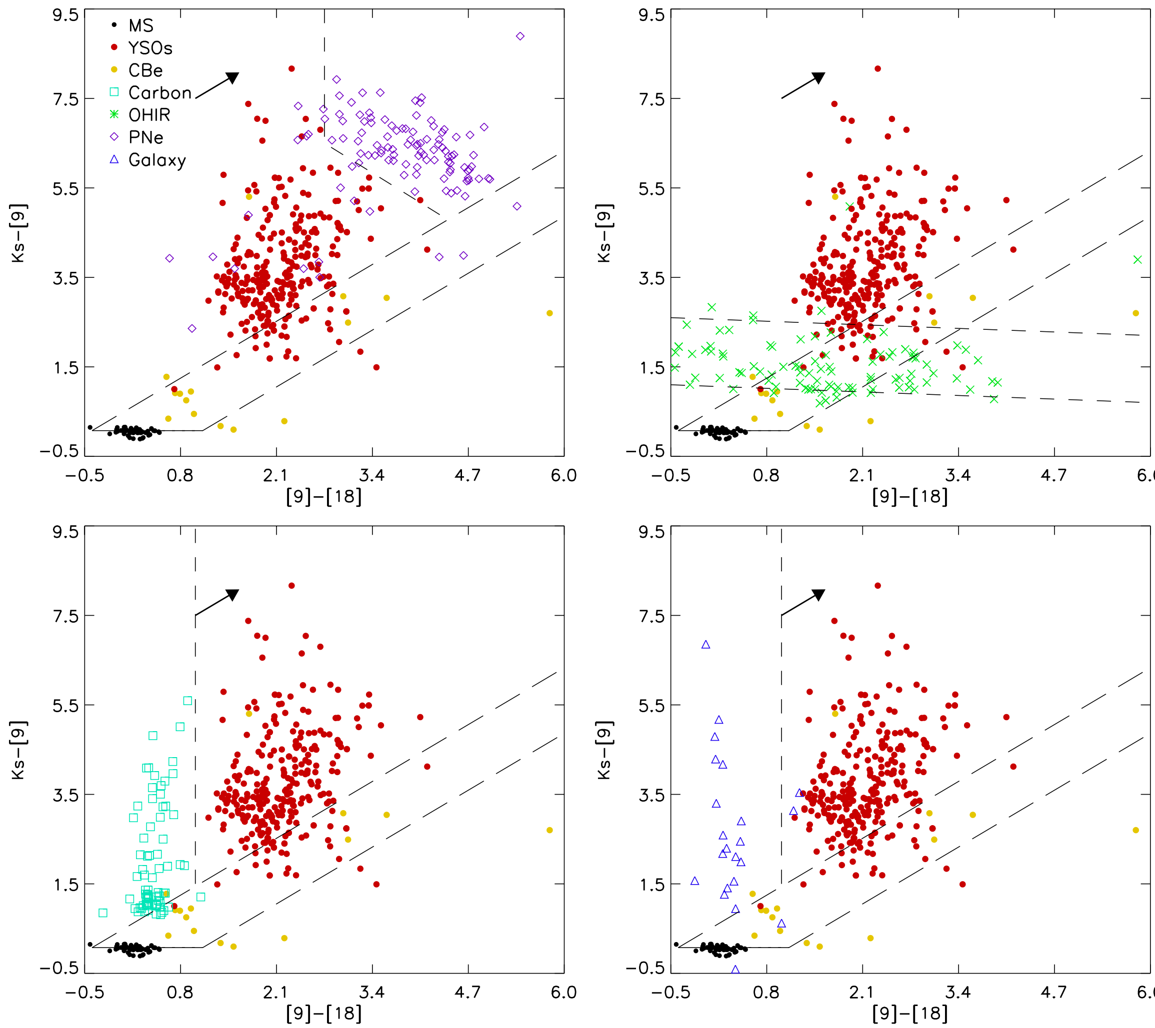

Figure 3. Distribution of contaminating sources in the K_S[9][18] C–C diagram. Short dashed lines show the regions from which we cut contaminants. The other lines and arrows are the same as those defined in Figure 2.

(A color version of this figure is available in the online journal.)

defined in an arbitrary manner as potentially the left edge of the distribution of CTTS and HAeBe in K_S[9][18], and the lower part of which is perpendicular to the reddening vector.

Figure 4 shows C–C diagrams of the second test sample sources, 28 Class I and 82 Class II sources, which are employed to discriminate between various types of YSOs at different evolutionary stages. As shown in Figure 4, almost all sample sources are found to be located to the right of the reddening band for normal stars in the JHK_S diagram, and to the right of the division lines defined above in the JK_S[9] and K_S[9][18] diagrams. However, unlike the distribution in the JHK_S diagram, a clear boundary between Class I and Class II sources exists in K_S[9][18] diagram, which indicates that mid-IR C–C diagrams can be used to distinguish YSOs at different evolutionary stages. Therefore, we defined a short dashed line as the division line between Class I and Class II sources in the K_S[9][18] C–C diagram.

Therefore, based on the distribution of the two test samples in various C–C diagrams, JHK_S C–C diagram can be used to distinguish different types of YSOs with different mass (HAeBe and CTTS), while mid-IR C–C diagrams are more efficient in the classification of YSOs at different evolutionary stages (Class I and Class II sources).

4. VERIFICATION OF THE SAMPLE SELECTION CRITERIA

To check the validity of the source selection criteria defined in the above section, we first performed a blind classification of archived IR sources toward IC 1396, a well-known H II region and active star-forming region. The field of study toward IC 1396 extends from 21^h28^m to 21^h52^m in right ascension and from 56° to 59° in declination, and centers on R.A. = $21^h40^m00^s$, decl. = 57°30′00″ (J2000.0), which is believed to encompass all the compact sub-clusters to their full extent (Huang & Li 2012). All archived sources of the 2MASS PSC in the field of study were cross-identified with the *AKARI* IRC catalog, which resulted in a sample of 637 sources. After removing possible contaminating sources, the sample sources were put onto the three C–C diagrams (Figure 5) and a detailed classification of the candidate YSOs were carried out based on the source selection criteria defined in this paper.

We define all objects as YSO candidates whose colors place them below the right line of the normal star reddening band in the JHK_S diagram and $H - K_S > 0.5$. Those sources are selected for intrinsic color excesses likely originating from emission of circumstellar dust. The color distinction helps to eliminate

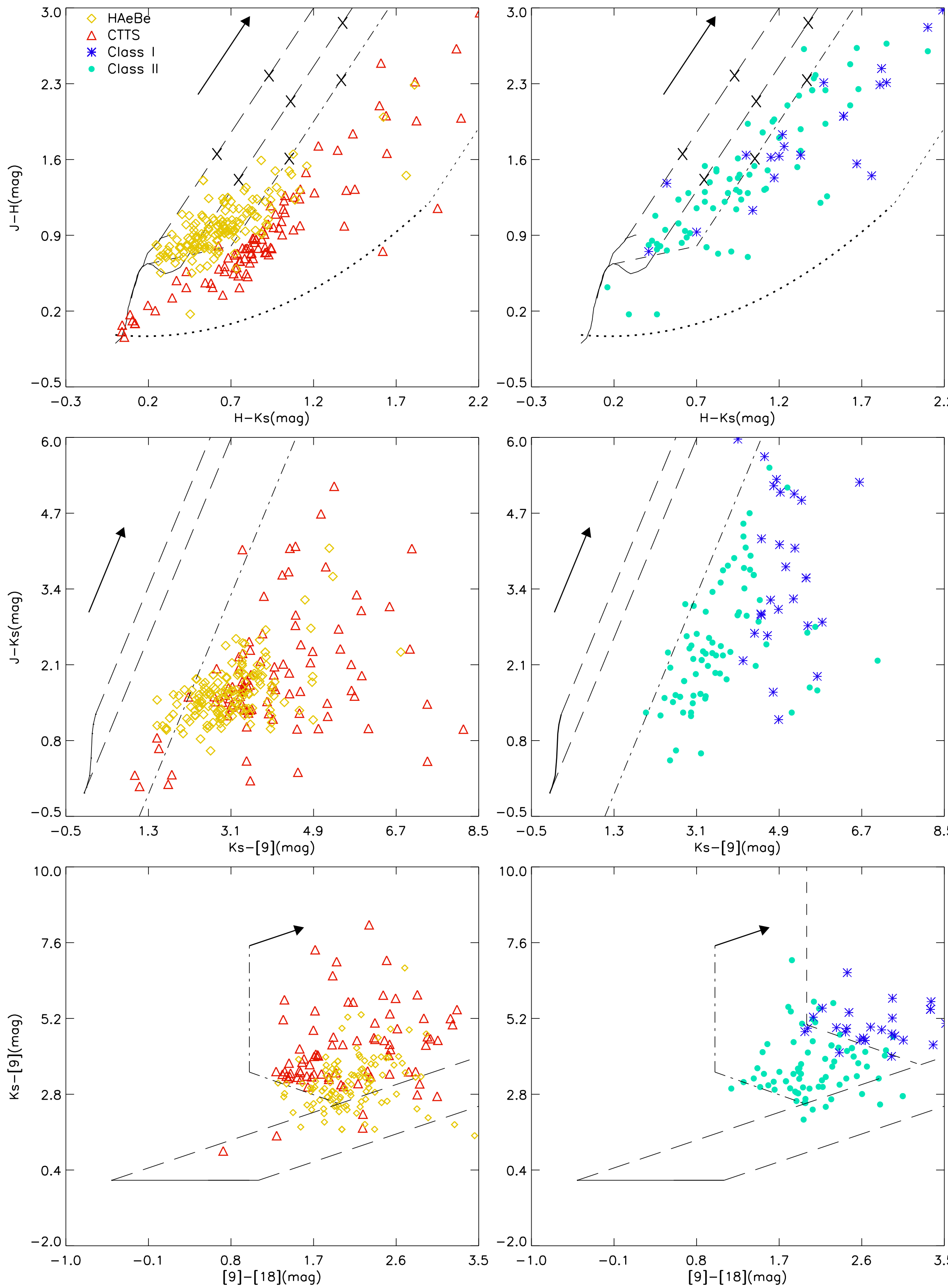

Figure 4. Distribution of the first test sample of HAeBe stars (Thé et al. 1994), and CTTSs from Herbig–Bell Catalogue (left), and the second test sample of Class I and Class II sources from Gutermuth et al. (2008, 2009; right) in C–C diagrams. Dot-dashed line, short dashed line, and dotted line in JHK_S indicate the division line between HAeBe and CTTS, the locus of dereddened TTS (Meyer et al. 1997), and the locus of dereddened HAeBe (Lada & Adams 1992), respectively. Dot-dashed lines in mid-IR C–C diagrams indicate the left boundary of YSOs. Short dashed line in K_S[9][18] diagram is the division line between Class I and Class II sources. Crosses were overplotted with an interval corresponding to 5 mag of visual extinction in JHK_S diagram. The other lines and arrows are the same as those defined in Figure 2.

(A color version of this figure is available in the online journal.)

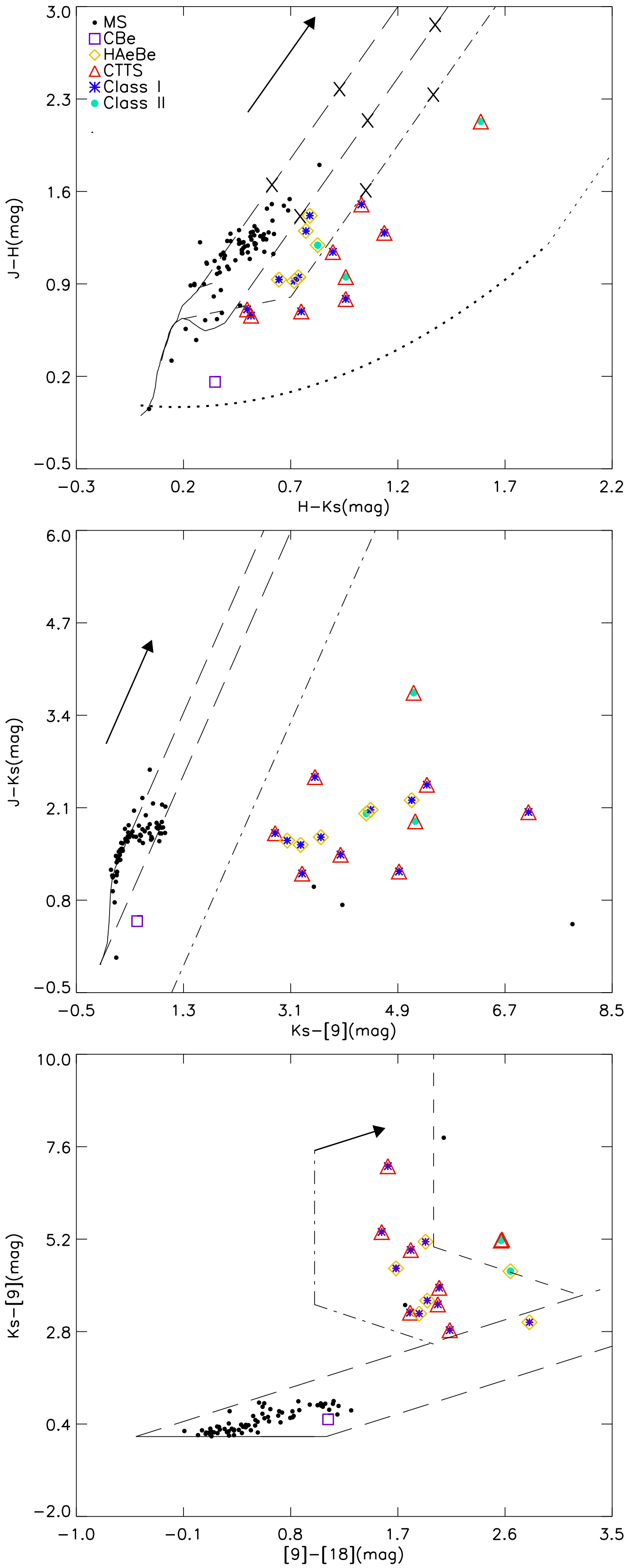

Figure 5. Blind classification of the candidate YSOs with excess emission in the IR toward IC 1396. The lines and arrows are the same as those defined in Figure 4.

(A color version of this figure is available in the online journal.)

a possible random distribution of foreground field stars without excluding potential cloud members that may also be widely distributed.

With our selection criteria, HAeBe and CTTSs were first selected in the JHK_S diagram, i.e., those located in between the reddening band and the dot-dashed line were taken as CTTSs and those to the right of the division line were taken as HAeBe. And then Class I sources and Class II sources were distinguished easily for that they are separated by the short dashed line in the K_S[9][18] diagram. Furthermore, a source was found matching well the location of CBe in the JHK_S diagram. It was taken as candidate CBe, which indeed show up in the expected loci in the JK_S[9] and K_S[9][18] diagrams. All results of the classification are presented in Table 3, which includes the sequence number of these sources, 2MASS PSC coordinates (J2000), EW[Hα], spectral types, classification based on optical spectra, SEDs, and our selection criteria.

To further verify the validity of the sources selection criteria, we have performed optical spectroscopy and SED fitting of sample sources.

4.1. Classification Based on Optical Spectra

Spectroscopic observations of all the sample sources with USNO R magnitudes brighter than 17.0 were performed and all optical spectra with Hα emission are listed in Figure 6 and arranged in order of spectral types.

Hα emission and lithium absorption are the two main features at optical wavelengths that can be used determine spectral types of YSOs. Combined with equivalent width measurements of Hα, EW[Hα], all the sources with spectral types earlier than F5 and Hα in emission were identified as HAeBe. CTTSs were selected based on the criteria that a CTTS shows EW[Hα] greater than 3 Å for K0–K5 stars, EW[Hα] greater than 10 Å for K7–M2.5 stars, EW[Hα] greater than 20 Å for M3–M5.5 stars, and EW[Hα] greater than 40 Å for M6–M7.5 stars (White & Basri 2003).

4.2. Classification Based on SED Fitting

We also tried to determine the evolutionary status of the sample sources based on their SEDs. A grid of 200,000 YSO models was developed (Robitaille et al. 2006), spanning a wide range of evolutionary stages for different stellar masses, to model the SED from optical to millimeter wavelengths. This archive transfer provides a linear regression tool that can select all model SEDs that fit the observed SED better than a specified χ^2 (Robitaille et al. 2006).

On the basis of the "four-staged" star formation scenario proposed by Shu et al. (1987), Lada (1987) developed a widely used classification scheme for YSOs, primarily based on their SEDs. With an evolutionary sequence from early type to late type, YSOs were classified into Class I to III. Robitaille et al. (2006) presented a classification scheme that is essentially analogous to the class scheme, but refers to the actual evolutionary stage of the object based on physical properties like disk mass and envelope accretion rate. However, in view of the differences between observable and physical properties, ages fitted by the tool and the slope of its near/mid-IR SED are our primary reference standard. Based on the results of SED fitting, we made an approximate classification of sample sources into TTS with disks (Class II) and heavily embedded protostars (Class I; Sicilia-Aguilar et al. 2006a). Class I refers

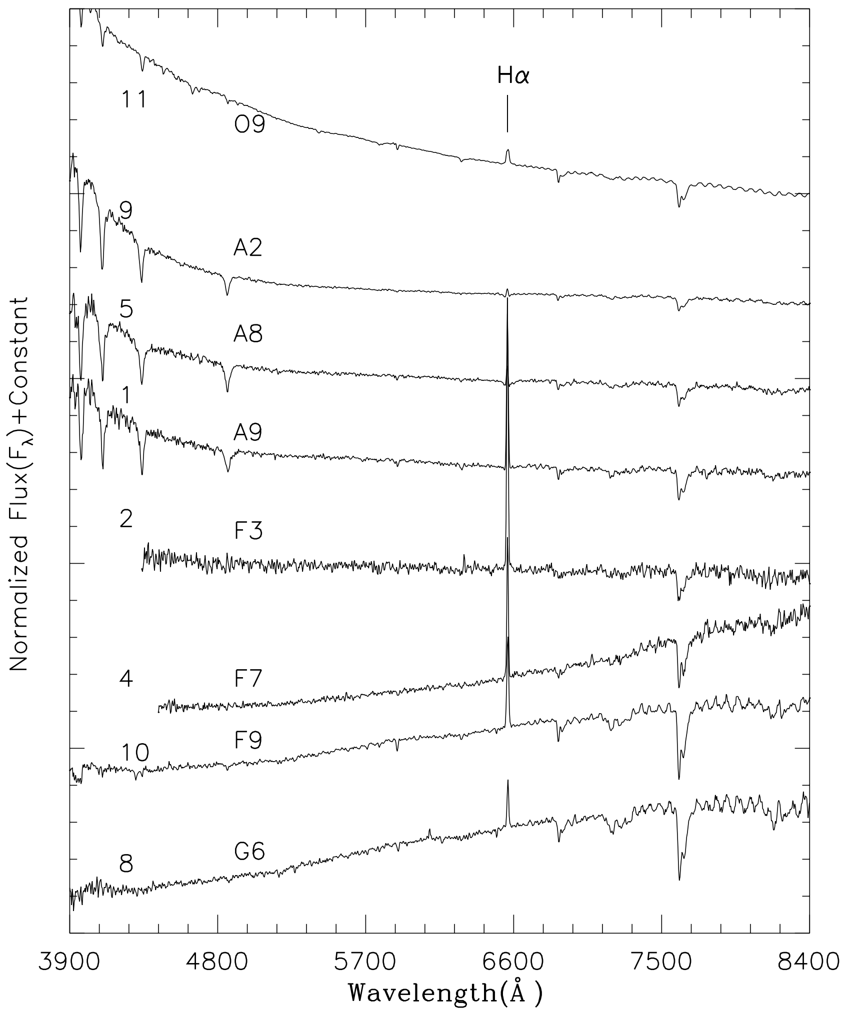

Figure 6. Optical spectra of the seven candidate YSOs and one CBe star with Hα emission toward IC 1396.

Table 3
Results of Identification and Classification of YSOs and CBe Toward IC 1396

ID	R.A.	Decl.	EW (Hα)	Sp.	Class			
	J2000		(Å)		Spectra	SED	Selection	Criteria
1[a]	21 30 22.8	+58 28 52	−40.5	A9	HAeBe	I	HAeBe	I
2	21 33 17.7	+57 48 13	−62.6	F3	HAeBe	II	HAeBe	II
3	21 33 49.3	+58 13 33	. . .	. . .	. . .	II	HAeBe	II
4[a]	21 34 19.6	+57 30 00	−45.1	F7	CTTS	I	CTTS	II
5[a]	21 35 19.1	+57 36 37	−6.98	A8	HAeBe	II	HAeBe	II
6	21 36 39.1	+57 29 53	. . .	. . .	. . .	II	HAeBe	II
7	21 36 46.3	+56 38 55	. . .	. . .	. . .	II	HAeBe	II
8[a]	21 36 49.4	+57 48 22	−6.52	G6	CTTS	II	CTTS	II
9[b]	21 38 08.3	+57 26 46	−5	A2	HAeBe	II	HAeBe	II
10[c]	21 38 17.2	+57 31 21	−14.5	F9	CTTS	II	CTTS	II
11	21 42 24.1	+57 44 09	−4.99	O9	CBe	. . .	CBe	. . .
12	21 45 02.2	+56 49 50	. . .	. . .	. . .	II	HAeBe	II
13	21 45 05.7	+57 11 37	. . .	. . .	. . .	II	CTTS	II
14	21 45 12.5	+57 10 49	. . .	. . .	. . .	I	HAeBe	I
15	21 45 36.7	+57 02 01	. . .	. . .	. . .	II	CTTS	II
16	21 46 00.0	+57 23 10	. . .	. . .	. . .	I	CTTS	I

Notes.
[a] Emission stars detected by Nakano et al. (2012).
[b] Member of Tr 37 identified by Sicilia-Aguilar et al. (2005).
[c] IC 1396 A: θ—identified as CTTS and member of Tr 37 by Sicilia-Aguilar et al. (2005, 2006b).

Table 4
Source Selection Criteria Defined for Various Types of YSOs and CBe Based on the C–C Diagrams Compiled Based on 2MASS and *AKARI*

Source		Definition of the Source Selection Criteria
HAeBe		$(J-H) - 2.3 \times (H-K_S) + 0.81 < 0$ or $(J-H) - 0.33 \times (H-K_S) - 0.57 < 0$
	and	$(K_S - S9W) + 1.023 \times (S9W - L18W) - 4.523 > 0$ $S9W - L18W > 1$
	or	$(J-K_S) - 1.9 \times (K_S - S9W) + 2.59 < 0$
CTTS		$-0.3 > (J-H) - 2.3 \times (H-K_S) > -0.81$ $(J-H) - 0.33 \times (H-K_S) - 0.57 > 0$
	and	$(K_S - S9W) + 1.023 \times (S9W - L18W) - 4.523 > 0$ $S9W - L18W > 1$
	or	$(J-K_S) - 1.9 \times (K_S - S9W) + 2.59 < 0$
Class I		$(J-H) - 2.3 \times (H-K_S) + 0.31 < 0$
	and	$(K_S - S9W) + 1.023 \times (S9W - L18W) - 7.046 > 0$ $S9W - L18W > 2$
Class II		$(J-H) - 2.3 \times (H-K_S) + 0.31 < 0$
	and	$4.523 < (K_S - S9W) + 1.023 \times (S9W - L18W) < 7.046$ $S9W - L18W > 1$
CBe		$(J-H) - 2.3 \times (H-K_S) + 0.3 < 0$ $(J-H) - 0.33 \times (H-K_S) - 0.57 < 0$
	and	$(K_S - S9W) - 0.978 \times (S9W - L18W) - 0.564 < 0$
	or	$(J-K_S) - 1.9 \times (K_S - S9W) + 2.59 > 0$

to those objects that have Age $\approx 10^5$ yr and Slope$_{\text{near/mid-IR}} > 0$, Class II refers to Age $\approx 10^6$ yr and Slope$_{\text{near/mid-IR}} \leqslant 0$.

As shown in Table 3, the classification of optical spectral and SEDs confirms the validity of our selection and classification criteria. Our selection and classification of excess emission sources are summarized in Table 4.

5. SUMMARY

We have presented in this paper new criteria for the selection and classification of various types of IR excess emission sources using 2MASS and *AKARI* colors. These include YSOs with different mass, i.e., HAeBe and CTTSs, Class I and Class II sources at different evolutionary status, and CBe. Based on their 2MASS and *AKARI* colors, high precision photometric data from the *Hipparcos* Catalog and the distribution of two test samples of known YSOs, different categories of IR excess emission sources were found to occupy well isolated loci in the color space.

A test study of the IR excess emission sources as candidate YSOs toward IC 1396 helps to verify the validity of the newly defined sources selection criteria. Optical identification and SED fitting of the candidate YSOs did confirm the efficient selection and classification of various types of excess emission sources based on the 2MASS and *AKARI* colors.

We appreciate very much the helpful comments and suggestions from the referee. This work employed data from the 2MASS, *AKARI*, the *Hipparcos* Catalog, and other databases. Our investigation is supported by funding from the National Natural Science Foundation of China through grant NSFC 11073027 and the Department of International Cooperation of the Ministry of Science and Technology of China through grant 2010DFA02710. The Mayall 4 m telescope at Kitt Peak National Observatory is a facility of the National Optical Astronomy Observatory, which is operated by the Association of Universities for Research in Astronomy, Inc. (AURA) under cooperative agreement with the National Science Foundation.

REFERENCES

Abt, H. A. 1986, ApJ, 304, 688
Acker, A., Ochsenbein, F., Stenholm, B., et al. 1994, yCat, 5084, 0
Draine, B. T. 2003, ARA&A, 41, 241
Gutermuth, R. A., Megeath, S. T., Myers, P. C., et al. 2009, ApJS, 184, 18
Gutermuth, R. A., Myers, P. C., Megeath, S. T., et al. 2008, ApJ, 674, 336
Huang, Y. F., & Li, J. Z. 2012, arXiv:1212.1530
Ishihara, D., Onaka, T., Kataza, H., et al. 2010, A&A, 514, A1
Ita, Y., Matsuura, M., Ishihara, D., et al. 2010, A&A, 514, A2
Jacoby, G. H., Hunter, D. A., & Christian, C. A. 1984, ApJS, 56, 257
Kawada, M., Baba, H., Barthel, P. D., et al. 2007, PASJ, 59, 389
Koenig, X. P., Leisawitz, D. T., Benford, D. J., et al. 2012, ApJ, 744, 130
Kun, M., Kiss, Z. T., & Balog, Z. 2008, in Handbook of Star Forming Regions: The Northern Sky, ed. B. Reipurth (San Francisco, CA: ASP), 136
Lada, C. J. 1987, in Proc. IAU Symp. 115, Star Forming Regions, ed. M. Peimbert & J. Jugaku (Dordredcht: Reidel), 1
Lada, C. J., & Adams, F. C. 1992, ApJ, 393, 278
Le Bertre, T., Tanaka, M., Yamamura, I., & Murakami, H. 2003, A&A, 403, 943
Li, J. Z., & Smith, M. D. 2005, A&A, 431, 925
Massey, P., Strobel, K., Barnes, J. V., & Anderson, E. 1988, ApJ, 328, 315
Meyer, M. R., Calvet, N., & Hillenbrand, L. A. 1997, AJ, 114, 288
Nakano, M., Sugitani, K., Watanabe, M., et al. 2012, AJ, 143, 61
Onaka, T., Matsuhara, H., Wada, T., et al. 2007, PASJ, 59, 401
Rieke, G. H., & Lebofsky, M. J. 1985, ApJ, 288, 618
Robitaille, T. P., Whitney, B. A., Indebetouw, R., Wood, K., & Denzmore, P. 2006, ApJS, 167, 256
Shu, F. H., Adams, F. C., & Lizano, S. 1987, ARA&A, 25, 23
Sicilia-Aguilar, A., Hartmann, L. W., Briceño, C., Muzerolle, J., & Calvet, N. 2004, AJ, 128, 805
Sicilia-Aguilar, A., Hartmann, L., Calvet, N., et al. 2006a, ApJ, 638, 897
Sicilia-Aguilar, A., Hartmann, L. W., Fürész, G., et al. 2006b, AJ, 132, 2135
Sicilia-Aguilar, A., Hartmann, L. W., Hernández, J., Briceño, C., & Calvet, N. 2005, AJ, 130, 188
Simonson, S. C., III 1968, ApJ, 154, 923
Takita, S., Kataza, H., Kitamura, Y., et al. 2010, A&A, 519, A83
Thé, P. S., de Winter, D., & Pérez, M. R. 1994, A&AS, 104, 315
White, R. J., & Basri, G. 2003, ApJ, 582, 1109